Editors' Suggestion | Featured in Physics

Surface Wave Electron Acceleration from Flat Foils at Parallel Laser Incidence

A. McCay,[1,2,*] A. McIlvenny,[1,†] A. Macchi,[3,4] L. Romagnani,[5] P. Martin,[1] O. Cavanagh,[1,6] D. P. Molloy,[1,7] L. Lancia,[5] T. Dzelzainis,[6] H. Ahmed,[6] J. Sarma,[1] S. Kar,[1] D. Margarone,[2,1] and M. Borghesi[1,‡]

[1]*Centre for Light-Matter Interactions, Queens University Belfast, Belfast BT7 1NN, United Kingdom*
[2]*ELI Beamlines Facility, The Extreme Light Infrastructure ERIC, Dolní Břežany 252 41, Czech Republic*
[3]*National Institute of Optics, National Research Council (CNR/INO), Adriano Gozzini Laboratory, 56124 Pisa, Italy*
[4]*Dipartimento di Fisica Enrico Fermi, Universitá di Pisa, Pisa, Italy*
[5]*LULI–CNRS, Ecole Polytechnique, CEA, Universite Paris-Saclay, F-91128 Palaiseau cedex, France*
[6]*Central Laser Facility, Rutherford Appleton Laboratory, Oxfordshire OX11 0QX, United Kingdom*
[7]*HB11 Energy Holdings Pty, Freshwater 2096, Australia*

(Received 10 December 2024; accepted 15 August 2025; published 1 October 2025)

The acceleration of electrons by surface plasma waves (SPWs) generated during the interaction of ultrashort, linearly polarized, and contrast-enhanced laser pulses at a peak intensity of $\sim 6 \times 10^{20}$ W cm^{-2} with flat, noncorrugated foils at parallel incidence (with respect to the target surface) is investigated. We experimentally demonstrate the generation of a collimated electron beam (< 0.6 mrad) with a non-Maxwellian spectrum, characterized by peaks at superponderomotive energies (30–36 MeV) and total charge $\sim$120 pC. Through particle-in-cell (PIC) simulations, we identify the $\mathbf{J} \times \mathbf{B}$ force at the front edge as the primary mechanism for injecting electrons into the SPW, where they are further accelerated. Furthermore, our simulation findings reveal that lateral surface contaminants influence SPW dynamics and give rise to a long-ranging plasmonic mode.

DOI: 10.1103/y29y-f63h

Surface plasmons (SPs) or surface plasma waves (SPWs) are electromagnetic excitations of free electrons that propagate along the boundary of a sharp material interface [1,2]. Generating SPWs with a laser pulse can result in substantial amplification and control of the electromagnetic field at the interface, with many applications in plasmonics [3,4]. SPWs from high-intensity laser-matter interactions [5] promise many benefits, such as producing ultrashort multi-MeV electron bunches [6,7], enhancing ion acceleration [8–10], generating high-flux x-rays [11,12] or high harmonics [13]. Electron acceleration is particularly effective as the phase velocity and longitudinal components of the surface plasmon enable the electrons to "surf" the plasma wave in a similar fashion to laser wakefield acceleration (LWFA) [14–18].

Previous experiments at relativistic intensities have used grating targets engraved with periodic modulations, enabling phase matching between the SPW and the laser pulse [6,7,10,19,20]. This is considered a necessary condition for an obliquely incident laser pulse. However, grating targets are expensive, difficult to manufacture, and prone to energy loss due to radiative scattering as the SPW propagates along the corrugated surface.

A recently proposed configuration, the "peeler acceleration" geometry [8], involves irradiating parallel to the surface of a thin flat foil. This eliminates the need for a grating because the phase velocity $\mathbf{v}_p$ mismatch between the laser and SPW is greatly reduced. Simulations have shown that this scheme can effectively excite a surface wave [8,9,21]. In this case, the laser will destructively interfere with the SPW when the accumulated phase difference $\Delta\phi$ becomes equal to π after propagating a distance $L_d \simeq N\lambda$, where λ is the laser wavelength and $N = n_e/n_c$ is the ratio between the electron and critical density, respectively. This dephasing length is, however, sufficiently long [8,9] to accelerate electrons to superponderomotive energies [22]. The electrons are accelerated mainly along the foil's surfaces by the longitudinal component of the SPW. In the limit $n_e \gg n_c$, the SPW's phase velocity $\mathbf{v}_p \simeq c$, and the fields are evanescent on both sides of the interface [23]. If an electron is injected exactly at a wave crest with a velocity equal to $\mathbf{v}_p$, it can achieve a maximum possible energy,

$$\mathcal{E}_{\max} = 4Nm_ec^2a_{\mathrm{SPW}}, \tag{1}$$

[*]Contact author: amccay06@qub.ac.uk
[†]Present address: Lawrence Berkeley National Laboratory, 1 Cyclotron Road, Berkeley, California, 94720, USA.
[‡]Contact author: m.borghesi@qub.ac.uk

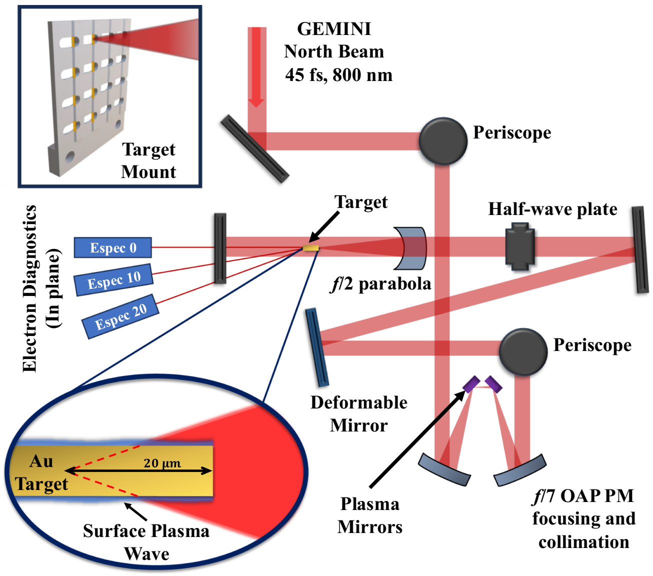

FIG. 1. Schematic of the experimental setup. Three high-resolution electron spectrometers were deployed at different angles 0°, 10°, and 20° (as labeled) with respect to the target surface. The bottom inset depicts the irradiating position with the laser pulse focused 20 μm beyond the front edge of a 6 μm gold target. The top inset shows the target matrix array used for parallel incidence shots.

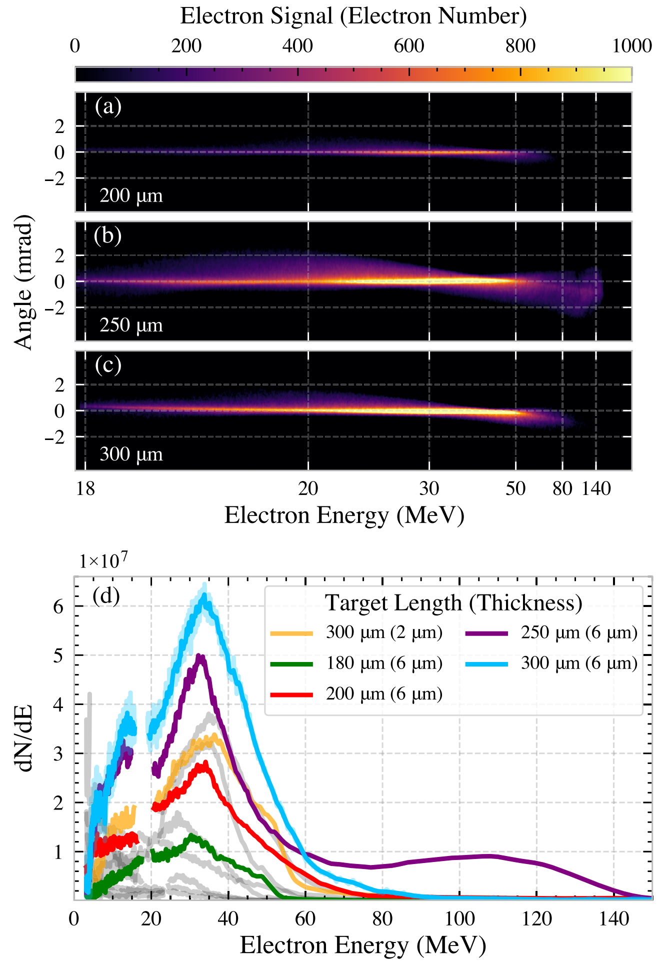

FIG. 2. (a)–(c) Raw BAS-TR image plate data from Espec 0 degrees. Electrons are generated from gold foils irradiated at parallel incidence using 200, 250, and 300 μm targets, respectively. (d) Electron spectra at 0 deg, smoothed using a 6σ Gaussian filter. Several representative shots for target lengths ranging from 180 to 300 μm are highlighted, while others are plotted in light gray to indicate shot-to-shot variations. Gaps around 17 MeV correspond to the electron spectrometer arrangement, specifically the separation between two image plates.

where $a_{\mathrm{SPW}} = (e/m_e \omega c) E_{\mathrm{SPW}}$ and E_{SPW} is the longitudinal field amplitude [12].

In this Letter, we report the experimental demonstration of high-energy electron acceleration by surface plasma waves excited on flat, noncorrugated thin foils. The electron beams exhibit low divergence, with a non-Maxwellian spectrum characterized by a pronounced peak at superponderomotive energies. Multidimensional particle-in-cell (PIC) simulations [24], conducted under conditions closely resembling those of the experiment, indicate that the electrons emitted from the rear target edge are injected into the SPW by the $\mathbf{J} \times \mathbf{B}$ force [25] at the front edge and are further accelerated along the target surface by the SPW. The impact of naturally occurring lateral surface contamination on extending the propagation of the plasma wave and enhancing the electron energies is also examined. The findings in this Letter provide key understandings for advancing high-field plasmonics by enabling the generation of SPs and their exploitation for electron acceleration without the need for complex targets.

The experiment was carried out using the Gemini laser system at the Rutherford Appleton Laboratory, UK. A double plasma mirror (DPM) setup was implemented for temporal pulse cleaning [26–28] to ensure a sharp density gradient between the target and vacuum. With the DPM deployed, the laser delivered approximately 6 J on target in a 45 fs full width at half maximum (FWHM) pulse with a central wavelength $\lambda = 80$ nm. The P-polarized beam was focused on the target at parallel incidence with an $f/2$ off axis parabola producing a ∼2.7 μm FWHM Gaussian focal spot and a peak intensity of $\sim 6 \times 10^{20}$ W cm^{-2}. A deformable mirror (DM) was implemented to correct for higher-order aberrations. To test the mechanism's dependence on polarization, a half-wave plate was placed in the beam path between the DM and the $f/2$ parabola. The main diagnostics included three electron spectrometers (Espec), each equipped with BAS-TR image plate (IP) detectors [29]. These were positioned at 0°, 10°, and 20° relative to the laser axis, with horizontal acceptance angles of approximately 21, 14, and 3 mrad, respectively. Gold targets with lengths in the range of $100 - 300$ μm were used with the beam focused 20 μm beyond the front edge, which in turn determines the effective spot size at the front surface and parallel surfaces (see Fig. 1).

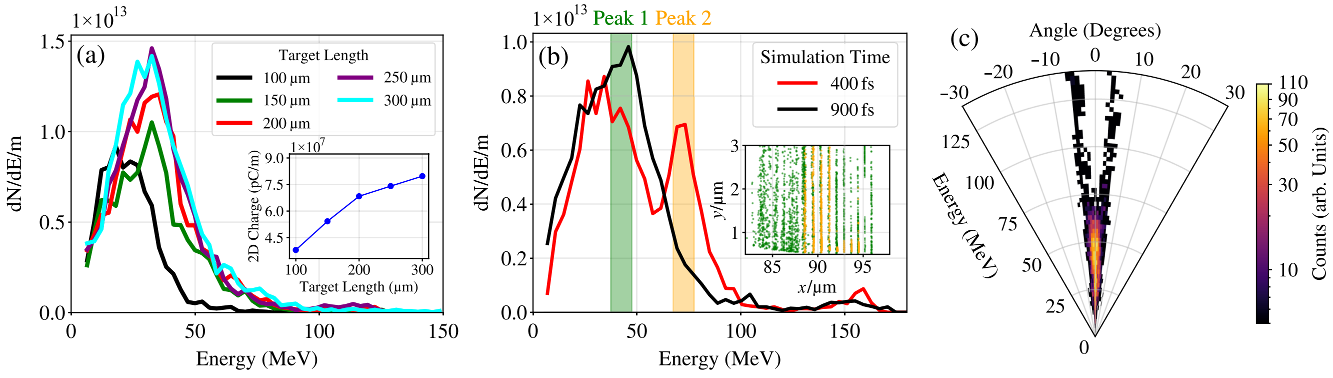

FIG. 3. (a) 2D simulated electron spectra at different values of target lengths taken 100 fs after exiting into vacuum. Particles were selected within a 20 μm slice. The inset shows the linear electron charge density vs target length. (b) Energy spectrum of electrons selected within the final spectrum for 250 μm target at 400 fs and 900 fs, respectively. Peaks 1 and 2 indicate electrons selected at 400 fs for Fig. 4, with an inset showing these electrons trapped in an SPW. (c) Polar plot of the angular distribution of the tracked electrons emitted from the rear edge of a 250 μm target.

The angular and energy distributions of electrons emitted from flat gold foils irradiated at parallel incidence are presented in Figs. 2(a)–2(c), as measured by the zero-degree electron spectrometer. For targets exceeding 200 μm in length, electron beams remain collimated along the laser axis, with a divergence of 0.6 mrad (full width at $1/e^2$ maximum) at the spectral peak, and an average divergence of 2.2 ± 0.4 mrad over the 17–150 MeV energy range. During parallel incidence shots, only a low flux of electrons with energies on the order of the ponderomotive energy $\varepsilon_p \sim 6$ MeV were observed on the 10- and 20-degree spectrometers.

The electron spectra obtained on the zero-degree Espec for a target length scan with *P*-polarized pulses are shown in Fig. 2(d). A non-Maxwellian distribution was consistently observed in each spectrum examined, with a prominent peak in the 30–36 MeV range with amplitude increasing with the target length. Targets with lengths greater than 300 μm were longer than the mount and were not self-supporting; thus, results from such shots were inconsistent due to alignment issues. While most spectra exhibited cut-off energies of 60–80 MeV, on one occasion, a second broad peak with lower amplitude and energies extending up to 140 MeV was observed. In general, the charge accelerated in the electron beam was estimated to be $Q_{Avg} \simeq 120 \pm 8$ pC. Decreasing the thickness from 6 to 2 μm resulted in a decrease in electron flux to $\sim 72 \pm 5$ pC, as highlighted in Fig. 2(d) for a 300 μm long target. Shots employing S-polarized pulses (250 μm by 5 μm targets) led to a large reduction of flux with a thermal spectrum and cutoff energy of 4–6 MeV.

The low energies and flux in the *S*-polarized shots reinforce the interpretation of electron acceleration by SPWs, as surface plasmon excitation necessitates *P*-polarized light [1,30].

The spectral peak observed in the *P*-polarization shots indicates that as the electrons traverse the target surface they synchronize with the SPW and settle into a relatively narrow energy range, forming a narrow band bunch. This peak is consistently observed within a similar energy range across all target lengths, suggesting that each target exceeds the maximum acceleration length.

The results obtained at the two different thicknesses are particularly noteworthy because both target thicknesses greatly exceed the skin depth. Assuming all electrons are continuously "peeled" from within the skin layer along the lateral surfaces, one would expect similar charge accumulation across different target thicknesses. However, the observed increase in electron flux with thicker targets suggests that electron injection is largely influenced by the conditions at the front edge of the target and that the available surface area for injection is a critical factor in determining the total charge.

To support and interpret the data, we performed 2D particle-in-cell (PIC) simulations using the fully relativistic EPOCH code [24], under conditions similar to the experiment. The target comprised Au^{51+} ions neutralized by electrons at 100 n_c, with 10 n_c H^+ layers of varying thicknesses on both lateral surfaces and the rear, representing typical experimental contamination. As typically the rising edge of the laser pulse removes front-layer contaminants [31], this layer was omitted. The target was irradiated at parallel incidence by an idealized 45 fs pulse with a 2.71 μm diameter (both Gaussian FWHM), focused 20 μm beyond the target edge. Simulations used a grid with $\Delta x =$ 15 nm and $\Delta y = 10$ nm, extending from $[-30\ \mu\text{m}, 30\ \mu\text{m}]$ along y and $[-20\ \mu\text{m}, \text{Target length} + 100\ \mu\text{m}]$ along x, with the laser propagating in x. Initially, the simulation contained 400 particles per cell for electrons and protons and 200 particles per cell for gold. Time zero corresponds to the pulse entering the domain at $x = -20$ μm.

Figure 3(a) shows the simulated electron spectra for 1 μm thick gold targets at various lengths with 50 nm contaminant layers. To simulate the Espec detector, we sample the electrons ejected from the rear edge by taking a ± 10 μm slice along the y direction, as SPW-accelerated electrons are predominantly emitted parallel to the target's surface. We observe the same spectral profile and trend as in the experiment with the electron flux increasing with the target length [see inset of Fig. 3(a)]. We estimate the electron charge in a real 3D geometry to be in the range of 110–220 pC by multiplying the linear charge density by the pulse FWHM diameter. Shown in Fig. 3(b) is the temporal evolution of the electrons for the 250 μm target at two separate time steps when the electrons trapped within the SPW are 90 μm along the target (400 fs) and when they reach the end of the target (900 fs). The electron spectra initially form two distinct peaks at different energies. During the interaction, the extra length allows the lower-energy electrons (Peak 1) located at the leading and trailing edges of the SPW to be accelerated further. Meanwhile, the higher-energy electrons (Peak 2) situated near the center of the SPW are decelerated as the field decays, causing the two peaks to merge.

As seen in Fig. 3(c), for long targets, nearly all accelerated electrons are contained within a $\pm 10°$ window, with the majority of the flux directed along the laser axis. This supports the experimental data, where we observed a collimated electron beam at 0° Espec and no high-energy electrons on the 10° and 20° Especs. There are two electron bunches with energies > 80 MeV that are directed off axis compared to the region of highest flux. Our diagnostic arrangements would not capture these beamlets on typical shots due to their directionality and collimation, although they may be detected occasionally in case of slight misalignment, which may be the case for the shot with the 140 MeV cutoff shown in Fig. 2(d). We estimate the maximum theoretical electron energy using the simulated longitudinal field $E_{\mathrm{SPW}} = 3.4 \times 10^{12}$ V m^{-1}, corresponding to $a_{\mathrm{SPW}} = 0.85$. For a 100 n_c target, we obtain $\mathcal{E}_{\max} = 174$ MeV, as given by Eq. (1), which is consistent with the highest energy observed in the off axis jets. However, most electrons also experience some transverse deflection, which may cause them to leave the accelerating region. In previous grating-based experiments, the final energy agreed reasonably with $\mathcal{E}_{\max}/4$ [6,12], which equates to $\simeq 43$ MeV in our simulations.

The key factor contributing to the flux increase in longer targets is the reduced divergence of electrons in Peak 2 from Fig. 3(b), resulting in more electrons detected within the slice and, thus, captured by the experimental Espec. This phenomenon is illustrated in Fig. 4 when tracking electrons within the two selected spectral regions. For shorter targets, the spectrum exhibits the double peak shape at the end of the target, where the electrons in Peak 2 interact with the EM field diffracted from the edge. At this point, the SPW dissipates its energy and excites strong plasma oscillations. These fields accelerate the electrons off axis at large angles (see Video 1 in Supplemental Material [32]). The overall effect diminishes with longer targets because both the trailing electron bunch and the SPW are weaker at the edge.

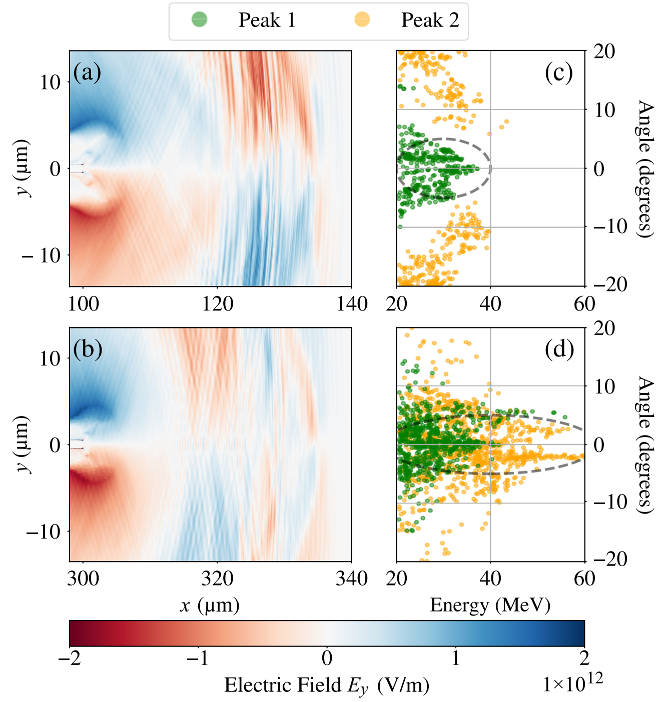

FIG. 4. Cycle averaged electric field component E_y with tracked electrons. (a) 100 μm target at 530 fs. (b) 300 μm target at 1200 fs. (c),(d) Indicate the angular distribution of electrons selected from Peak 1 and Peak 2 at 400 fs indicated in Fig. 3(b). Dashed ellipses show electrons that would be detected on Espec 0.

The simulations further reveal the origin of the electrons contributing to the spectral shape. Figure 5 shows particle tracking results, where electrons within the spectrum are traced back to their source and overlaid on the electron density and the E_y component of the electric field. We see that the detected electrons originate from the front edge, where they are injected and subsequently trapped in the SPWs excited on both sides of the target with a wavelength of $\simeq\lambda_L$ (since $\omega_p \gg \omega_L$) and a phase shift of $\lambda_L/2$ between the two sides.

In this instance, the dominant injection mechanism is the $\mathbf{J} \times \mathbf{B}$ force, accelerating electrons with velocity and propagation direction closely matching that of the SPW [33]. The $\mathbf{J} \times \mathbf{B}$ injection mechanism at the front edge is consistent with the experimental results shown in Fig. 2(d), where thicker targets tend to accumulate more charge. The double-peaked spectral shape in Fig. 3(b) can be attributed to the injection at the front edge, with the higher energy electrons injected by the laser pulse peak and the lower energy electrons injected by the leading and trailing edge of the pulse (see inset).

Since the injected electrons are confined to the lateral surfaces, their dynamics can be affected by contamination commonly present under experimental conditions. In

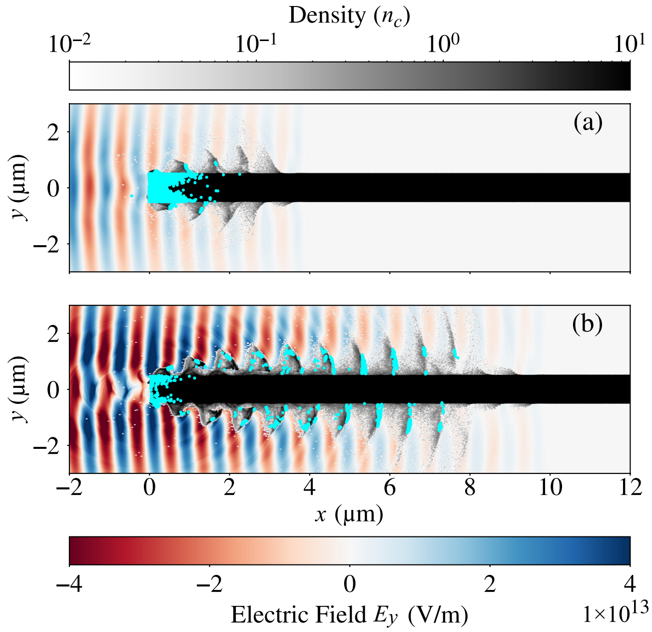

FIG. 5. Particle tracking simulation snapshots of a parallel laser-solid interaction, showing the tracked electrons from the spectrum in Fig. 3(a) (cyan) overlaid with the electric field component E_y and electron density (gray) at times (a) $t = 80$ fs and (b) $t = 100$ fs.

simulations without these contaminants, the same non-Maxwellian spectrum does not appear, and a thermal spectrum is observed (see Supplemental Material [32]). With the presence of contaminants, surface plasmonic modes are excited at the different interfaces of this multilayer system (metal-contaminant interface and contaminant-vacuum interface) [1]. In the contaminant layer, the field profile dips as the two evanescent waves couple. The field gradients on either side (plasma and vacuum) are shallower compared to a standard SPW. As a result, the fields of this plasmonic mode extend farther from the surface helping trap electrons within the SPW by reducing lateral deflection and exhibiting reduced electron heating in the transverse direction [12]. The simulations suggest the decay rate of the SPW field strength along the propagation direction (x axis) is reduced by the presence of a lateral surface contaminant, making the configuration more favorable for electron acceleration. In plasmonics, this is known as a *long-ranging surface plasma wave* (LRSPW), which has less confinement and, therefore, longer propagation lengths [34–36].

In conclusion, our Letter demonstrates the excitation of surface plasma waves on flat, noncorrugated foils at relativistic intensities. This interaction produces a collimated electron beam featuring a non-Maxwellian spectrum with peaks at superponderomotive energies. We establish that the SPW is the primary mechanism responsible for the high-energy electron acceleration, while identifying the $\mathbf{J}\times\mathbf{B}$ force at the front edge as the dominant driver for injecting electrons into the SPW phase and highlighting the impact of lateral surface contaminants on SPW dynamics. The electron acceleration scheme reported here, while less efficient than established mechanisms such as laser wakefield, advances significantly the capabilities of acceleration processes employing solid targets, including SPW-based schemes relying on complex grating structures. The compact nature of the required setup may benefit scientific experiments where introducing the long focal length optics required for wakefield acceleration may be impractical, due to space constrains, e.g., in multibeam arrangements. Finally, as the peeler's geometry has been originally introduced in the context of an advanced proton acceleration scheme [8], the demonstration of efficient electron beam production is an important milestone, as an intermediate step toward achieving the enhanced proton beam characteristics (high energy, high flux, narrow-band spectrum) observed in simulations [8,9].

Acknowledgments—The authors would like to thank the GEMINI staff and the engineering and target fabrication groups at the CLF for their support. The authors acknowledge funding from EPSRC [Grant No. EP/P010059/1], the IMPULSE project by the European Union Framework Program for Research and Innovation Horizon 2020 under Grant Agreement No. 871161, and the UHDPULSE EMPIR program cofinanced by the Participating States and from the European Union's Horizon 2020 research and innovation program. Through using the EPOCH code, this work has also in part been supported by EPSRC Grants No. EP/G054950/1, No. EP/G056803/1, No. EP/G055165/1, and No. EP/M022463/1. The authors also acknowledge the computing resources provided by the Kelvin High-Performance Computing cluster at Queen's University Belfast.

Data availability—The data that support the findings of this Letter are openly available [37].

[1] S. Maier, Plasmonics: Fundamentals and applications, 10.1007/0-387-37825-1 (2007).

[2] J. Pitarke, V. Silkin, E. Chulkov, and P. Echenique, Theory of surface plasmons and surface-plasmon polaritons, Rep. Prog. Phys. **70**, 1 (2006).

[3] R. E. Rottmayer, S. Batra, D. Buechel, W. A. Challener, J. Hohlfeld, Y. Kubota, L. Li, B. Lu, C. Mihalcea, K. Mountfield *et al.*, Heat-assisted magnetic recording, IEEE Trans. Magn. **42**, 2417 (2006).

[4] A. G. Brolo, Plasmonics for future biosensors, Nat. Photonics **6**, 709 (2012).

[5] A. Macchi, M. Borghesi, and M. Passoni, Ion acceleration by superintense laser-plasma interaction, Rev. Mod. Phys. **85**, 751 (2013).

[6] L. Fedeli, A. Sgattoni, G. Cantono, D. Garzella, F. Réau, I. Prencipe, M. Passoni, M. Raynaud, M. Květoň, J. Proska *et al.*, Electron acceleration by relativistic surface plasmons

in laser-grating interaction, Phys. Rev. Lett. **116**, 015001 (2016).

[7] G.-y. Hu, A.-l. Lei, W.-t. Wang, X. Wang, L.-g. Huang, J.-w. Wang, Y. Xu, J.-s. Liu, W. Yu, B.-f. Shen *et al.*, Collimated hot electron jets generated from subwavelength grating targets irradiated by intense short-pulse laser, Phys. Plasmas **17**, 033109 (2010).

[8] X. F. Shen, A. Pukhov, and B. Qiao, Monoenergetic high-energy ion source via femtosecond laser interacting with a microtape, Phys. Rev. X **11**, 041002 (2021).

[9] J. Sarma, A. McIlvenny, N. Das, M. Borghesi, and A. Macchi, Surface plasmon-driven electron and proton acceleration without grating coupling, New J. Phys. **24**, 073023 (2022).

[10] S. Bagchi, P. Prem Kiran, W.-M. Wang, Z. Sheng, M. Bhuyan, M. Krishnamurthy, and G. Ravindra Kumar, Surface-plasmon-enhanced MeV ions from femtosecond laser irradiated, periodically modulated surfaces, Phys. Plasmas **19**, 030703 (2012).

[11] X. Shen, A. Pukhov, and B. Qiao, High-flux bright x-ray source from femtosecond laser-irradiated microtapes, Commun. Phys. **7**, 84 (2024).

[12] A. Macchi, G. Cantono, L. Fedeli, F. Pisani, and T. Ceccotti, Extreme high field plasmonics: Electron acceleration and XUV harmonic generation from ultrashort surface plasmons, Phys. Plasmas **26**, 042114 (2019).

[13] L. Fedeli, A. Sgattoni, G. Cantono, and A. Macchi, Relativistic surface plasmon enhanced harmonic generation from gratings, Appl. Phys. Lett. **110**, 051103 (2017).

[14] T. Tajima and J. M. Dawson, Laser electron accelerator, Phys. Rev. Lett. **43**, 267 (1979).

[15] S. P. Mangles, C. Murphy, Z. Najmudin, A. G. R. Thomas, J. Collier, A. E. Dangor, E. Divall, P. Foster, J. Gallacher, C. Hooker *et al.*, Monoenergetic beams of relativistic electrons from intense laser–plasma interactions, Nature (London) **431**, 535 (2004).

[16] J. Faure, Y. Glinec, A. Pukhov, S. Kiselev, S. Gordienko, E. Lefebvre, J.-P. Rousseau, F. Burgy, and V. Malka, A laser–plasma accelerator producing monoenergetic electron beams, Nature (London) **431**, 541 (2004).

[17] E. Esarey, C. B. Schroeder, and W. P. Leemans, Physics of laser-driven plasma-based electron accelerators, Rev. Mod. Phys. **81**, 1229 (2009).

[18] M. Raynaud, J. Kupersztych, C. Riconda, J. Adam, and A. Heron, Strongly enhanced laser absorption and electron acceleration via resonant excitation of surface plasma waves, Phys. Plasmas **14**, 092702 (2007).

[19] G. Cantono, L. Fedeli, A. Sgattoni, A. Denoeud, L. Chopineau, F. Réau, T. Ceccotti, and A. Macchi, Extreme ultraviolet beam enhancement by relativistic surface plasmons, Phys. Rev. Lett. **120**, 264803 (2018).

[20] X. M. Zhu, R. Prasad, M. Swantusch, B. Aurand, A. A. Andreev, O. Willi, and M. Cerchez, Relativistic electron acceleration by surface plasma waves excited with high intensity laser pulses, High Power Laser Sci. Eng. **8**, e15 (2020).

[21] S. Marini, M. Grech, P. S. Kleij, M. Raynaud, and C. Riconda, Electron acceleration by laser plasma wedge interaction, Phys. Rev. Res. **5**, 013115 (2023).

[22] S. C. Wilks, W. L. Kruer, M. Tabak, and A. B. Langdon, Absorption of ultra-intense laser pulses, Phys. Rev. Lett. **69**, 1383 (1992).

[23] L. D. Landau, E. M. Lifshitz, L. P. Pitaevskii, J. S. Bell, M. J. Kearsley, and J. B. Sykes, *Electrodynamics of Continuous Media*, 2nd ed., Course of Theoretical Physics Vol. 8 (Elsevier, Amsterdam, Netherlands, 1984), Chap. X, Sec. 88.

[24] T. Arber, K. Bennett, C. Brady, A. Lawrence-Douglas, M. Ramsay, N. J. Sircombe, P. Gillies, R. Evans, H. Schmitz, A. Bell *et al.*, Contemporary particle-in-cell approach to laser-plasma modelling, Plasma Phys. Controlled Fusion **57**, 113001 (2015).

[25] W. L. Kruer and K. Estabrook, J × b heating by very intense laser light, Phys. Fluids **28**, 430 (1985).

[26] B. Dromey, S. Kar, M. Zepf, and P. Foster, The plasma mirror—A subpicosecond optical switch for ultrahigh power lasers, Rev. Sci. Instrum. **75**, 645 (2004).

[27] A. Lévy, T. Ceccotti, P. d'Oliveira, F. Réau, M. Perdrix, F. Quéré, P. Monot, M. Bougeard, H. Lagadec, P. Martin *et al.*, Double plasma mirror for ultrahigh temporal contrast ultraintense laser pulses, Opt. Lett. **32**, 310 (2007).

[28] C. Thaury, F. Quere, J.-P. Geindre, A. Levy, T. Ceccotti, P. Monot, M. Bougeard, F. Réau, P. d'Oliveira, P. Audebert *et al.*, Plasma mirrors for ultrahigh-intensity optics, Nat. Phys. **3**, 424 (2007).

[29] N. Rabhi, K. Bohacek, D. Batani, G. Boutoux, J.-E. Ducret, E. Guillaume, K. Jakubowska, C. Thaury, and I. Thfoin, Calibration of imaging plates to electrons between 40 and 180 MeV, Rev. Sci. Instrum. **87**, 053306 (2016).

[30] A. Sgattoni, L. Fedeli, G. Cantono, T. Ceccotti, and A. Macchi, High field plasmonics and laser-plasma acceleration in solid targets, Plasma Phys. Controlled Fusion **58**, 014004 (2015).

[31] A. McIlvenny, D. Doria, L. Romagnani, H. Ahmed, N. Booth, E. J. Ditter, O. C. Ettlinger, G. S. Hicks, P. Martin, G. G. Scott, S. D. R. Williamson, A. Macchi, P. McKenna, Z. Najmudin, D. Neely, S. Kar, and M. Borghesi, Selective ion acceleration by intense radiation pressure, Phys. Rev. Lett. **127**, 194801 (2021).

[32] See Supplemental Material at http://link.aps.org/supplemental/10.1103/y29y-f63h for additional information on the experimental and simulation data.

[33] C. Riconda, M. Raynaud, T. Vialis, and M. Grech, Simple scalings for various regimes of electron acceleration in surface plasma waves, Phys. Plasmas **22**, 073103 (2015).

[34] D. Sarid, Long-range surface-plasma waves on very thin metal films, Phys. Rev. Lett. **47**, 1927 (1981).

[35] B. Prade, J. Y. Vinet, and A. Mysyrowicz, Guided optical waves in planar heterostructures with negative dielectric constant, Phys. Rev. B **44**, 13556 (1991).

[36] P. Berini, Long-range surface plasmon polaritons, Adv. Opt. Photonics **1**, 484 (2009).

[37] A. McCay *et al.*, Data for "Surface Wave Electron Acceleration from Flat Foils at Parallel Laser Incidence", Queen's University Belfast. PRL_McCay_data(.zip), README(.txt) (2025), 10.17034/ba65ff12-d460-4408-8038-38e9f482244a.